

Nucleotides Increase the Internal Flexibility of Filaments of Dephosphorylated *Acanthamoeba* Myosin II*

(Received for publication, December 8, 1995, and in revised form, February 28, 1996)

M. Jolanta Redowicz, Edward D. Korn, and Donald C. Rau§

From the Laboratory of Cell Biology, NHLBI and the ‡Office of the Director, NIDDK, National Institutes of Health, Bethesda, Maryland 20892

The actin-activated Mg^{2+} -ATPase activity of *Acanthamoeba* myosin II minifilaments is dependent both on Mg^{2+} concentration and on the state of phosphorylation of three serine sites at the C-terminal end of the heavy chains. Previous electric birefringence experiments on minifilaments showed a large dependence of signal amplitude on the phosphorylation state and Mg^{2+} concentration, consistent with large changes in filament flexibility. These observations suggested that minifilament stiffness was important for function. We now report that the binding of nucleotides to dephosphorylated minifilaments at Mg^{2+} concentrations needed for optimal activity increases the flexibility by about 10-fold, as inferred from the birefringence signal amplitude increase. An increase in flexibility with nucleotide binding is not observed for dephosphorylated minifilaments at lower Mg^{2+} concentrations or for phosphorylated minifilaments at any Mg^{2+} concentration examined. The relaxation times for minifilament rotations that are sensitive to the conformation myosin heads are also observed to depend on phosphorylation, Mg^{2+} concentration, and nucleotide binding. These latter experiments indicate that the actin-activated Mg^{2+} -ATPase activity of *Acanthamoeba* myosin II correlates with both changes in myosin head conformation and the ability of minifilaments to cycle between stiff and flexible conformations coupled to nucleotide binding and release.

The heavy chain component of the multiple members of the myosin superfamily share a highly homologous head (but with sufficient sequence differences to allow their classification into 10 or 11 families) connected to highly variable tails (1). The ATP- and actin-binding sites, actin-activated Mg^{2+} -ATPase activity, and *in vitro* motility activity all reside in the conserved head domain. The tail is generally thought to determine the supramolecular organization of the myosins and their associations with specific cell structures and organelles. For example, the two N-terminal heads of type II myosin heavy chains are attached to a long rodlike C-terminal tail that self-associates into an α -helical coiled-coil and subsequently assemble into a bipolar filament (the heavy chains of other myosin classes either remain monomeric or form dimers but do not form filaments).

The heavy chains of most class II myosins can be proteolytically cleaved to light meromyosin (LMM),¹ the C-terminal end

of the α -helical, coiled-coil rod, and heavy meromyosin (HMM), the N-terminal portion of the α -helical, coiled-coil rod with its two attached globular heads (2). LMM retains the filament-forming properties of native myosin II, and HMM retains all of the catalytic activity and *in vitro* motility activity. HMM can be further proteolyzed to two monomers of subfragment 1 (S1), a single globular head with an α -helical C-terminal tail, and subfragment 2 (S2), the α -helical, coiled-coil portion of HMM. The individual S1 fragments retain most of the properties of HMM.

Class II myosins contain two pairs of light chains, essential light chains (ELC) and regulatory light chains (RLC), with one of each pair attached to the helical tail of each S1 domain (3). Some (molluscan) native type II myosins are activated by direct binding of Ca^{2+} to the ELC and others (smooth muscle, vertebrate nonmuscle, and *Dictyostelium*) by phosphorylation of the RLC (4). The light chains stabilize the helical tail of S1 (3, 5), and removal of the light chains or the helical tail of S1 greatly reduces the ability of S1 to move actin filaments in an *in vitro* motility assay (6), but neither the light chains nor the helical tail of S1 are necessary for maximal actin-activated Mg^{2+} -ATPase activity of S1. These data are consistent with the most recent structural model of the contractile cycle derived from x-ray crystallography of S1; conformational changes in the globular portion of S1 resulting from the binding and hydrolysis of ATP are transmitted through the ELC and generate a rotational movement of the helical tail of S1 (7). This model was supported by recent experiments that demonstrate tilting of the light chain region of the myosin head during muscle contraction (8).

It seems likely, however, that the head and tail domains of class II myosins are not as functionally independent as the foregoing brief summary might imply. For example, the myosin superfamily can be grouped into essentially the same classes based on the overall structure of their tails (1), suggesting co-evolution of the head and tail domains that would presumably result from their functional interactions. Moreover, the actin-activated Mg^{2+} -ATPase activities of S1 from both ELC-regulated and RLC-regulated muscle myosins are unregulated (whereas HMM is regulated), suggesting that at least a portion of the tails is necessary for the appropriate coupling of S1 head and light chain conformations (4).

Acanthamoeba myosin II provides a striking example of the functional interaction of the head and tail regions of a myosin II; both the actin-activated Mg^{2+} -ATPase activity and the *in vitro* motility activity of minifilaments of *Acanthamoeba* myosin II are inactivated by phosphorylation of 3 serine residues in a short (29 amino acids), nonhelical tail piece at the C-terminal tip of the α -helical, coiled-coil rod (9, 10). Extensive experimen-

* The costs of publication of this article were defrayed in part by the payment of page charges. This article must therefore be hereby marked "advertisement" in accordance with 18 U.S.C. Section 1734 solely to indicate this fact.

§ To whom correspondence should be addressed: Bldg. 5, Rm. 405, National Institutes of Health, Bethesda, MD 20892. Tel.: 301-402-4698; Fax: 301-496-0825; E-mail: donrau@helix.nih.gov.

¹ The abbreviations used are: LMM, light meromyosin; ELC, essen-

tial light chain; HMM, heavy meromyosin; S1, subfragment 1; S2, subfragment 2; AMPPNP, 5'-adenylyl-imidodiphosphate; DTT, dithiothreitol; RLC, regulatory light chain.

tal data (11–13) show that the activity of each molecule in the filament depends not on its own phosphorylation state but on the level of phosphorylation of the filament as a whole. This led to the hypothesis that the state of phosphorylation at the tip of the tail affects the conformation of the hinge region at the HMM-LMM junction in the tails of adjacent molecules in the minifilament and, thereby, the interactions with F-actin of the S1 heads at the ends of the HMM arms. Electric birefringence studies on chymotrysin-treated *Acanthamoeba* myosin II parallel dimers (14) indeed indicated that the tip of the tail of one monomer was in close proximity to the hinge region of the other.

Further electric birefringence experiments showed that the signals from minifilaments are fundamentally different from the monomer and parallel dimer signals; they were interpreted as being due to a coupling of internal motions, bending or flexing, and alignment in an electric field (15). Furthermore, these studies indicated that the stiffness of *Acanthamoeba* myosin II minifilaments is correlated with their actin-activated Mg^{2+} -ATPase activity. Filaments of dephosphorylated myosin II stiffen dramatically between 1 and 4 mM Mg^{2+} . The optimal concentration for both catalytic and *in vitro* motility activities for dephosphorylated minifilaments occurs at about 4–5 mM Mg^{2+} . In contrast, filaments of phosphorylated myosin, which are inactive at all Mg^{2+} concentrations, remain flexible even at 4 mM Mg^{2+} .

Recent experiments (16) showing that binding of ATP to *Acanthamoeba* myosin II enhances the rate of papain cleavage of the heavy chain of monomers in the region corresponding to that which interacts with the ELC in chicken myosin II (3) are consistent with the proposal (7) that ATP induces conformational changes in S1. However, ATP also promotes papain cleavage within the C-terminal tail of phosphorylated minifilaments (16); this was not anticipated. We now investigate the effects of nucleotides on the flexibility of phosphorylated and dephosphorylated minifilaments. The electric birefringence signal amplitude of dephosphorylated minifilaments indicates that an order of magnitude increase in flexibility accompanies nucleotide binding at 4–5 mM Mg^{2+} but not at lower Mg^{2+} concentrations. Phosphorylated minifilaments remain flexible at all Mg^{2+} concentrations between 1 and 5 mM in the presence of nucleotide. In addition, over the same range of experimental conditions, differences in either the structure or orientation of S1 heads can be inferred from differences in relaxation times of the spinning rotational motions. These results demonstrate that a complex interplay among C-terminal phosphorylation state, Mg^{2+} concentration, and nucleotide binding determines minifilament flexibility and conformation and, ultimately, regulates enzymatic activity.

EXPERIMENTAL PROCEDURES

Myosin Preparations—*Acanthamoeba* myosin II was isolated (17) and dephosphorylated by potato acid phosphatase as described (18). One portion of the dephosphorylated myosin II was then phosphorylated with partially purified myosin II heavy chain kinase (19). Dephosphorylated and phosphorylated myosin II were separated from phosphatase and kinase, respectively, by Sepharose CL-4B gel filtration (13), dialyzed against 10 mM imidazole, pH 7.0, 0.1 M KCl, 1 mM DTT, 10% sucrose, concentrated against solid sucrose, and stored at 4 °C. The extent of heavy chain phosphorylation was quantified as described by Ganguly *et al.* (13). Routinely, the incorporation was 3–5 mol of phosphate/mol of myosin II. Myosin preparations were also characterized by their actin-activated Mg^{2+} -ATPase activities; only dephosphorylated myosin II that was maximally active at 4–5 mM $MgCl_2$ and phosphorylated myosin II that had minimal activity at 10 mM $MgCl_2$ (20) were used for further studies.

Myosin II stock solutions used in the electric birefringence experiments were extensively dialyzed against 2.5 mM imidazole (pH 7.0), 5 mM KCl, 1 mM DTT, and 50% sucrose. Final protein concentrations were 1–2 mg/ml. Samples used in electric birefringence experiments were

first adjusted to 1 mM KCl, 2 mM imidazole (pH 7.4), 1 mM DTT, and 5% sucrose. The $MgCl_2$ was added in aliquots, with mixing, to obtain the final Mg^{2+} concentration. Although no difference in signal was observed for adding nucleotide before Mg^{2+} , nucleotide was typically added last.

ATPase Assays— Mg^{2+} -ATPase activity was measured under the conditions used for the electric birefringence measurements. Briefly, dephosphorylated myosin II minifilaments were adjusted on ice to 1 mM KCl, 1 mM DTT, 2 mM imidazole (pH 7.4), 5% sucrose, and 10 μ g/ml myosin, with and without 15 μ M F-actin (21). Activities were measured from 0.5 μ M to 1 mM ATP in 4 mM $MgCl_2$ by measuring the release of ^{32}P from [γ - ^{32}P]ATP (22).

Electric Birefringence—The instrumentation used has been described elsewhere (14, 15). In brief, 632.8 nm light from a He-Ne laser (Uniphase, model 105–1) passes through a high quality Glan polarizing prism, oriented at 45 °C with respect to vertical. The orientation of myosin II minifilaments in an externally applied electric field is characterized by the angle of rotation, δ , of plane polarized light as it passes through the sample and a subsequent $\lambda/4$ retardation plate oriented with its slow axis perpendicular to the initial plane of polarization. The light then passes through a second analyzing Glan polarizing prism oriented slightly off perpendicular to the initial plane of polarization. The angle δ of rotation is determined from the change in light intensity detected by a high speed photodiode (EG&G HAD 1100A). To an excellent approximation,

$$\delta = \alpha \frac{\Delta I}{I_\alpha} \quad (\text{Eq. 1})$$

where α is the angle between polarizers relative to the crossed orientation (typically 1 °C), I_α is the output voltage from the photodiode and amplifier at the angle α (typically 1000 mV), and ΔI is the change in output voltage due to the birefringence of the oriented sample.

The relaxation times of the two birefringence components were extracted from the decay data by several methods. First, the relaxation time of the slow, negative birefringence component was determined directly from the slope of the semilog plot of signal intensity *versus* time at long times (>150 μ s after the end of the pulse) as illustrated in Fig. 5. The relaxation time of the fast, positive birefringence component was then determined from the slopes of semilog plots of signal *versus* time after subtracting the contribution of the slow component, as shown in Fig. 6. The entire decay curve was also fit to a double exponential function, and best fitting values for τ_{slow} and τ_{fast} were determined simultaneously. Finally, the birefringence decay was also analyzed using the Fortran program Contin (23, 24), which gives a spectrum of relaxation times from an inverse Laplace transform of the data. The average relaxation times determined by the three methods did not differ significantly. The slowly decaying component can be well fit by a single exponential. We are less certain that the positive birefringence component has only a single relaxation time. We report fast decay times as average values, $\langle \tau_{\text{fast}} \rangle$, to emphasize this point.

As previously noted, a major experimental limitation was a field-induced, time-dependent aggregation of minifilaments that occurred at Mg^{2+} concentrations above about 4–5 mM. High protein concentrations, extended signal averaging, long field pulses, or high field strengths led first to a slowly decaying tail in the birefringence signal and eventually to visibly clouded solutions. This aggregation was less of a problem at pH 7.4 used in these experiments than at pH 7.0, which we used previously (15). The decrease in signal amplitude for dephosphorylated minifilaments, however, requires higher Mg^{2+} concentrations at pH 7.4 than at 7.0. The previously reported signal amplitudes at 4 mM Mg^{2+} at pH 7.0 require 4.5–5 mM at pH 7.4, depending on the specific myosin preparation. To avoid aggregation but also to achieve maximal signal amplitude and signal to noise ratio standard conditions for the experiments reported here were a protein concentration of about 40 μ g/ml, a field strength $E \sim 1.2$ kV/cm, and a voltage pulse length of 140 μ s. Optical signals from a single sample were averaged over 32 pulses. Occasionally, much longer pulse lengths (~ 800 μ s) were used to ensure that more slowly relaxing birefringence components were not present. Signal amplitudes were also measured as a function of field strength, E , up to about 2 kV/cm to verify that δ scales with E^2 . Signal amplitudes were also observed to vary linearly with protein concentration up to about 100 μ g/ml.

Overview of the Electric Birefringence Signal from Minifilaments—Fig. 1 illustrates the general features of the electric birefringence signal of *Acanthamoeba* myosin II minifilaments reported previously (15). The overall signal is composed of at least two major components that are evident in the kinetics of both the signal rise when the electric field is applied (+ E) and the decay after the field is removed (– E): (i) a com-

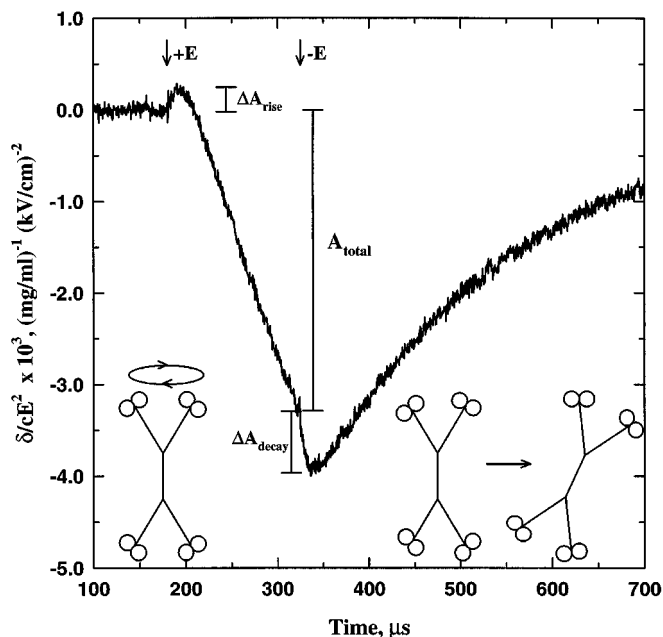


FIG. 1. A typical electric birefringence signal for minifilaments of dephosphorylated *Acanthamoeba* myosin II. Minifilaments at 40 $\mu\text{g/ml}$ were in 2 mM Mg^{2+} , 1 mM KCl, 2 mM imidazole (pH 7.4), 1 mM DTT, and 5% sucrose at 20 °C. The optical signal, shown normalized for field strength and myosin concentration and plotted as a function of time, is due to the orientation of minifilaments in an applied electric field, E , with the long filament axis aligned perpendicularly to the field. The square wave electric field pulse starts at 180 μs (relative to the start of data acquisition) and ends at 320 μs , as indicated by the arrows. The optical signal of both the build-up (with field on) and the decay (after field is removed) is the sum of at least two components, one with positive birefringence that relaxes much faster than the component with negative birefringence that dominates the signal amplitude. The fast, positive birefringence component is due to a spinning rotation about the minifilament long axis, illustrated in the lower left hand cartoon of a tetrameric, bipolar filament with two HMM arms (with S1 globular heads depicted as spheres at the ends of the S2 rods) extending in opposite directions from each end of a filament comprising four LMM segments. The more slowly relaxing, negative birefringence component is due to an end-over-end tumbling rotation of the minifilament, illustrated in the lower right. Each component is characterized by an amplitude, A , and a relaxation time, τ . The overall signal amplitude, A_{total} , and the ratio of the birefringence change at the maximum in the rise, ΔA_{rise} , to the birefringence change at the minimum in the decay, ΔA_{decay} , are predicted to depend on the flexibility of the minifilaments.

paratively small signal with positive birefringence that appears immediately after the field is applied and decays rapidly when the field is removed, and (ii) a much larger signal with negative birefringence that relaxes with much slower kinetics. Each component can be characterized by an amplitude, A , and relaxation time, τ .

Compared with this complicated set of signals from minifilaments, the electric birefringence signals from *Acanthamoeba* myosin II monomers and parallel dimers (14) are straightforward and provide a basis for understanding the minifilament signals. A large permanent dipole from the distribution of charged amino acids (25) extends over the HMM region of *Acanthamoeba* myosin II. The alignment of this permanent dipole in an electric field results in positive birefringence signals for monomers and parallel dimers, indicating that molecules are orienting with their long axes parallel to the field. Qualitatively similar positive birefringence signals are seen for skeletal muscle myosin HMM and S1 heads (26, 27). Unperturbed minifilaments, however, have no net dipole moment due to the symmetry of the structure. A dipole moment can still be induced if the HMM arms can bend or flex in the direction of the applied field (28). An internal flexibility of synthetic muscle myosin filaments was observed previously using spectroscopically labeled S1 heads (29–31).

The dipole moment resulting from the bending or flexing motions of the HMM can couple through the applied field to the two fundamental rotational modes of the minifilament illustrated in Fig. 1: (i) the spinning rotation about the long axis and (ii) the end-over-end tumbling of

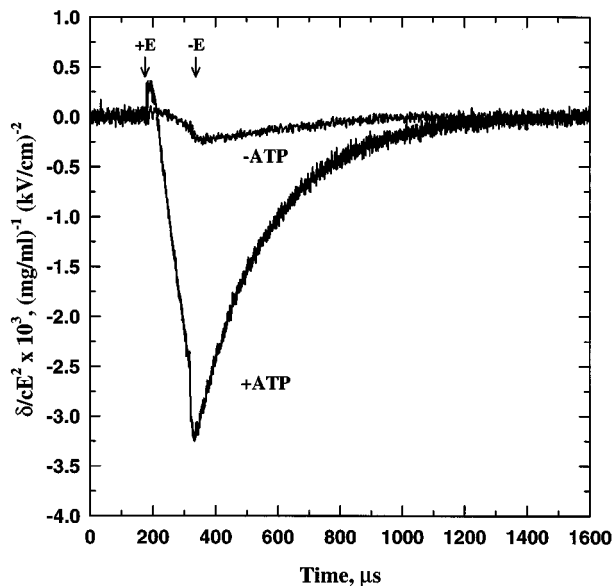


FIG. 2. The effect of added ATP on the electric birefringence signal amplitude for dephosphorylated minifilaments in 5 mM Mg^{2+} at 20 °C. The optical signal is shown normalized for field strength and protein concentration, δ/cE^2 , as in Fig. 1. The start and end of the 140- μs long electric field pulse are indicated by the arrows. The increase in signal amplitude was about 10-fold with ATP binding. In addition to the Mg^{2+} , the samples also contained 1 mM KCl, 2 mM imidazole (pH 7.4), 1 mM DTT, 5% sucrose, and 40–50 $\mu\text{g/ml}$ protein. The added ATP concentration was 250 μM .

the long axis, which correspond to the fast and slow relaxation kinetics of the positive and negative birefringence components, respectively. For average orientations of the HMM arms that are predominately parallel to the minifilament long axis and for small bending perturbations (low field strengths), the electric field induced dipole moment is predicted to be perpendicular to the long axis. The negative birefringence of the slowly relaxing component results from this unusual perpendicular orientation of the dipole and optical axes. The relaxation time of this component, τ_{slow} , is dependent on the distribution of mass along the minifilament axis. In practice, it is most sensitive to the number of monomers in the minifilament and the spacings between them. The positive birefringence signal is due to a component of the optical anisotropy that is perpendicular to the long axis (parallel to the dipole axis). We previously estimated, for example, that a 20 ° angle between the HMM axis and the minifilament axis is sufficient to account for the observed ratio of component amplitudes, $A_{\text{fast}}/A_{\text{slow}}$. The S2 rods of HMM are expected to contribute more substantially to the optical signal than the globular S1 heads (26). The decay time of the spinning rotation that relaxes this positive birefringence component, $\langle\tau_{\text{fast}}\rangle$, depends on the distribution of all mass perpendicular to the long axis.

The magnitude of the total birefringence signal is a measure of the bending force constant or the stiffness resisting internal HMM motions. Additionally, because the internal motions that create the net dipole moment couple with the rotations of the minifilament only in the rise part of the birefringence curve the ratio $-\Delta A_{\text{rise}}/\Delta A_{\text{decay}}$ (see Fig. 1) is also expected to vary with the kinetics of the bending or flexing and thus is also connected to the stiffness.

RESULTS

Effect of Nucleotides on Signal Amplitude—Fig. 2 shows the effect of ATP on signal amplitudes in 5 mM Mg^{2+} . As found previously (15), the amplitudes of both the positive and negative birefringence components of dephosphorylated myosin II minifilaments in the absence of nucleotide are much smaller in 5 mM Mg^{2+} than in 2 mM Mg^{2+} (compare the upper curve in Fig. 2 to Fig. 1). The addition of ATP to dephosphorylated minifilaments in 5 mM Mg^{2+} increased the signal amplitude to a magnitude similar to that observed at the lower concentration of Mg^{2+} in the absence of nucleotide (compare the lower curve in Fig. 2 with Fig. 1).

The direction and magnitude of the effect of ATP on signal

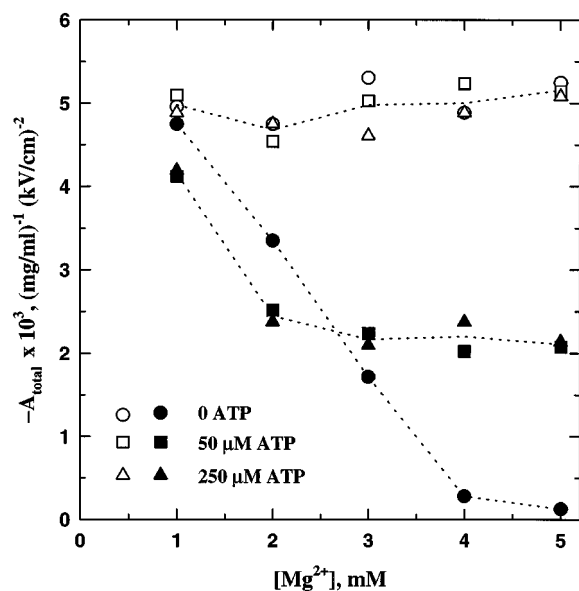


FIG. 3. The effect of ATP on the electric birefringence signal amplitude as a function of Mg^{2+} concentration. The total birefringence signal amplitude, $-A_{total}$, normalized by applied field strength and protein concentration, after a 140- μs electric field pulse is shown for both phosphorylated (*open symbols*) and dephosphorylated (*solid symbols*) minifilaments. The ATP concentrations were: 0 (*circles*), 50 (*squares*), and 250 μM (*triangles*). Other solution conditions were as described in the legend to Fig. 2.

amplitude varied with the Mg^{2+} concentration and with myosin phosphorylation, as shown in Fig. 3. At 1 and 2 mM Mg^{2+} , the total signal amplitude of dephosphorylated minifilaments decreased somewhat with added ATP (*filled symbols*), whereas above about 3 mM Mg^{2+} , ATP increased the total signal amplitude. This reversal in the effect of ATP reflects the 20–25-fold decrease in signal amplitude between 1 and 5 mM Mg^{2+} in the absence of ATP but comparatively constant amplitude in its presence. In contrast, the birefringence signal amplitude of phosphorylated minifilaments was not affected either by the Mg^{2+} concentration, as observed previously (15), or by the presence of ATP (Fig. 3, *open symbols*).

The nucleotide concentration dependence of the amplitude of the birefringence signal for dephosphorylated myosin II minifilaments at 4.5 mM Mg^{2+} is shown in Fig. 4 for ATP, ADP, and the nonhydrolyzable ATP analogue AMPPNP. The protein concentration in these experiments was $\sim 0.1 \mu M$ in myosin II monomers or $\sim 0.2 \mu M$ in S1 heads. The lowest concentration of AMPPNP used, 0.4 μM , was sufficient to achieve essentially the maximal increase in signal amplitude (Fig. 4, *squares*). Even when the protein concentration was increased to $\sim 0.35 \mu M$ S1, an AMPPNP concentration of 0.4 μM was still sufficient to obtain the maximal effect, *i.e.*, even when the concentration of heads and AMPPNP were approximately equal (data not shown). Similarly, the addition of an approximately equimolar concentration of AMPPNP was sufficient to obtain the maximum decrease in the amplitude of the birefringence signal at 2 mM Mg^{2+} (data not shown). These data indicate that the K_d for AMPPNP binding is smaller than 0.2–0.4 μM , which is consistent with the K_d of $\sim 0.09 \mu M$ that was estimated by differential scanning calorimetry.²

In contrast to the stoichiometric effect of AMPPNP, the increase in birefringence signal amplitude with added ATP or ADP was more consistent with a titration of binding sites between 0 and 4 μM nucleotide (Fig. 4). No further increase in

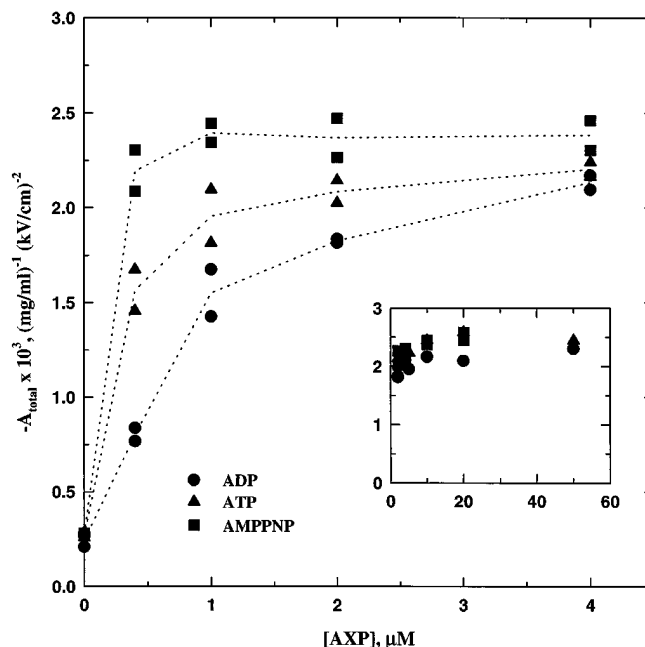


FIG. 4. The dependence of the electric birefringence signal amplitude for dephosphorylated minifilaments at 4.5 mM Mg^{2+} on nucleotide concentration. The field strength and protein concentration normalized optical signal amplitude at 20 °C is plotted as a function of nucleotide concentration for ATP (\blacktriangle), ADP (\bullet), and AMPPNP (\blacksquare). The *inset* shows signal amplitudes for nucleotide concentrations up to 50 μM . Other solution conditions were as described in the legend to Fig. 2. The 40–50- $\mu g/ml$ protein concentration corresponds to $\sim 0.2 \mu M$ S1.

signal amplitude was observed between 5 and 50 μM ADP or ATP (Fig. 4, *inset*). Consistent with this behavior, increasing the myosin concentration from ~ 0.2 to $\sim 0.35 \mu M$ S1 significantly decreased the observed signal amplitude at 0.4 μM ADP and to a somewhat greater extent also at 0.4 μM ATP, but it had a much smaller effect at ADP and ATP concentrations higher than 1 μM (data not shown).

From the birefringence data, the K_d for ADP is ~ 1 –2 μM , a not unreasonable value because ADP would be expected to bind to myosin more weakly than AMPPNP. In contrast to expectations, however, ATP also appears to bind to the myosin II minifilaments more weakly than AMPPNP. But, because the actin-independent Mg^{2+} -ATPase activity of dephosphorylated myosin II under the experimental conditions used for the electric birefringence measurements is ~ 5 –10 $\times 10^{-3} s^{-1}$, most of the ATP (for initial concentrations up to $\sim 4 \mu M$) was likely hydrolyzed to ADP during the course of a typical 30–60-min experiment. Thus, the high K_d estimated for ATP binding might actually have been for ADP binding instead.

Relaxation Kinetics—The relaxation time of the negative birefringence component of dephosphorylated minifilaments was insensitive to the total signal amplitude both in the presence and the absence of nucleotide. Fig. 5 shows a comparison of the signal decay for minifilaments in 3 and 4.5 mM Mg^{2+} without added nucleotide and in 4.5 mM Mg^{2+} with 5 μM AMPPNP. The average relaxation time, τ_{slow} , was $235 \pm 15 \mu s$, corrected to water viscosity at 20 °C. The relaxation time of the slow component was also unchanged in 50 μM AMPPNP, 250 μM ATP, and 5 and 50 μM ADP (data not shown). Relaxation times of the negative birefringence component with and without added nucleotides at two Mg^{2+} concentrations are summarized in Table I for both dephosphorylated and phosphorylated myosin II minifilaments. In general, the slow relaxation time is insensitive to myosin phosphorylation, Mg^{2+} concentration, and nucleotide binding.

² M. Zolkiewski, M. J. Redowicz, E. D. Korn, and A. Ginsburg, unpublished observation.

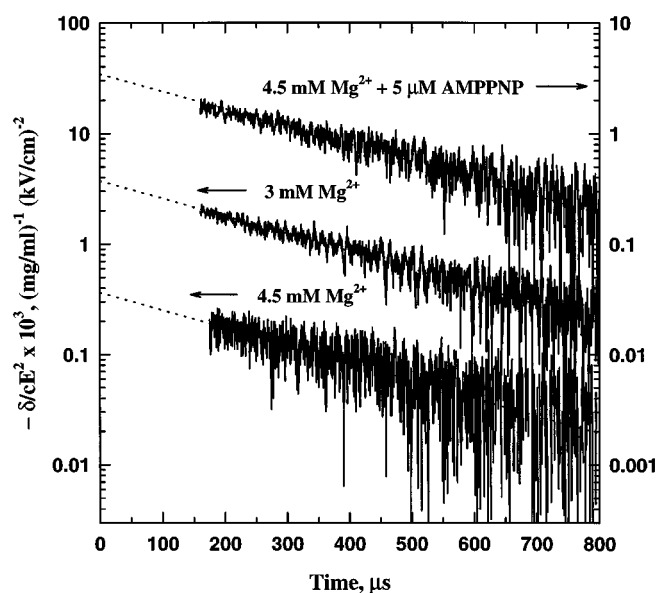


FIG. 5. The effect of Mg^{2+} and nucleotide on the decay kinetics of the slow, negative birefringence component of dephosphorylated minifilaments. Semilog plots of the optical signal, normalized for field strength and protein concentration, versus time, with $t = 0$ set at the end of the applied pulse, are shown for minifilaments in 3, 4.5, and 4.5 mM Mg^{2+} with 5 μM AMPPNP. The dashed lines are the best linear fits to the data. The arrows indicate the ordinate appropriate for each decay curve. The signal amplitudes for minifilaments in 3 mM Mg^{2+} (left ordinate) and in 4.5 mM Mg^{2+} with 5 μM AMPPNP (right ordinate) were about equal; the signal intensity of minifilaments in 4.5 mM Mg^{2+} was about a factor of 10 smaller (left ordinate). Other solution conditions were as described in the legend to Fig. 2.

In contrast, the relaxation time of the fast, positive birefringence component was markedly dependent on both Mg^{2+} and nucleotide. Fig. 6 illustrates the ~ 3.5 -fold difference in the average fast component relaxation times, $\langle \tau_{fast} \rangle$, for dephosphorylated minifilaments in 4.5 mM Mg^{2+} with 5 μM ADP (45 μs) and in 3 mM Mg^{2+} without added nucleotide (12 μs). This difference in relaxation times was observed even though the total signal amplitudes for these two experimental conditions were comparable. Average fast component relaxation times for other conditions of nucleotide and Mg^{2+} concentration are summarized in Table I for dephosphorylated and phosphorylated minifilaments. The increase in the fast relaxation time for dephosphorylated minifilaments depended on the nucleotide species bound, ranging from 40–45 μs with bound ADP to 25–30 μs with AMPPNP and 20–25 μs with ATP. In contrast, the average fast relaxation time for phosphorylated minifilaments actually decreased somewhat with added ATP from 12–13 to 8–9 μs .

Effect of Nucleotide on Other Birefringence Parameters—Table I summarizes the effect of added nucleotides (ATP, ADP, and AMPPNP) at two Mg^{2+} concentrations on several parameters extracted from the birefringence experiment for both dephosphorylated and phosphorylated minifilaments. In addition to the total signal amplitude, A_{total} , and the relaxation times of the positive and negative birefringence components, $\langle \tau_{fast} \rangle$ and τ_{slow} , already discussed, two other parameters are also given in Table I. As noted previously (15), the difference in total signal amplitude between dephosphorylated and phosphorylated minifilaments at 4.5–5 mM Mg^{2+} was accompanied by a difference in $\Delta A_{rise}/\Delta A_{decay}$ (cf. Fig. 1) and a small difference in A_{fast}/A_{slow} . The nucleotide-dependent increase in A_{total} for dephosphorylated myosin II at 4–5 mM Mg^{2+} was also coupled to a decrease in the ratio $-\Delta A_{rise}/\Delta A_{decay}$ from about 0.4 to 0.2. In contrast, the small increase in the ratio of the

positive to negative birefringence amplitudes, A_{fast}/A_{slow} , of dephosphorylated minifilaments as the Mg^{2+} concentration was increased from 3 to 4.5 mM was not reversed by adding nucleotide. In fact, the binding of ADP slightly increased this ratio even further. As with the average fast relaxation time, A_{fast}/A_{slow} is not tightly linked to signal amplitude and flexibility.

DISCUSSION

Structural Implications of the Change in Total Signal Amplitude—We previously reported that the electric birefringence signal amplitude of dephosphorylated *Acanthamoeba* myosin II minifilaments decreases significantly as the Mg^{2+} is increased from 1 to 4 mM, i.e., to the concentration range necessary for optimal expression of actin-activated Mg^{2+} -ATPase activity. We now find that the total signal amplitude is also dependent on nucleotide binding at the higher Mg^{2+} concentrations. Upon the addition of low concentrations of ADP, ATP, or AMPPNP, A_{total} increases about 10-fold at 4–5 mM Mg^{2+} . This increase in signal amplitude is not simply due to an increase in the dipole moment that might accompany binding of a charged ligand because nucleotides cause a decrease in the signal amplitude for dephosphorylated minifilaments at Mg^{2+} concentrations between 1 and about 3 mM. Moreover, nucleotides have no effect on the signal amplitude of phosphorylated minifilaments at 1–5 mM Mg^{2+} concentration even though nucleotides bind as well to phosphorylated minifilaments as to dephosphorylated minifilaments.

The absence of a significant change in the relaxation time of the slow component, τ_{slow} , upon the addition of nucleotides to dephosphorylated minifilaments further indicates that nucleotide binding does not cause a large change in the overall structure of the minifilament. The basic structure, the number of monomers, the repeat distance between monomers, and the length of the central bare zone, is not significantly different in the presence or the absence of nucleotide. In particular, there is no evidence for aggregation, consistent with analytical ultracentrifugation data (16). Therefore, the order of magnitude of increase in total signal amplitude with nucleotide binding at 4–5 mM Mg^{2+} most probably results from a substantial increase in the flexibility of minifilaments. The decrease of $-\Delta A_{rise}/\Delta A_{decay}$ at 4–5 mM Mg^{2+} from 0.4 to 0.2 (Table I) with added nucleotide is also consistent with an increase in flexibility (28). This ratio will depend on stiffness through the kinetics of the bending motion and a value of ~ 0.2 is characteristic of other conditions that give approximately the same signal amplitude.

Because nucleotide binding can either increase or decrease the signal amplitude, depending on the Mg^{2+} concentration, the effects of nucleotides and Mg^{2+} are neither independent nor simply additive. Rather, both likely regulate the flexibility of either the same or tightly coupled sites. We previously suggested that the bending site was at the HMM-LMM junction rather than at the S1-S2 junction or an elastic flexing of the S2 rod itself based on the estimated bending kinetics extracted from $-\Delta A_{rise}/\Delta A_{decay}$. This has been confirmed by more recent experiments on *Acanthamoeba* myosin II rods and rods in which the bend at the HMM-LMM junction has been removed or modified by amino acid substitution. The results demonstrate that the S1 heads are not necessary to obtain full signal amplitude but that the “native” HMM-LMM bend is essential (32). The electric birefringence signal of native *Acanthamoeba* myosin II minifilaments almost certainly arises from bending at the HMM-LMM junction. Preliminary data³ also show that

³ D. C. Rau, M. J. Redowicz, E. D. Korn, and J. A. Hammer III, unpublished observation.

TABLE I
Electric birefringence amplitude and relaxation time parameters for dephosphorylated and phosphorylated *Acanthamoeba myosin II* minifilaments for different conditions of Mg^{2+} concentration and nucleotide binding

The electric birefringence experiments were done at 20 °C and in 1 mM KCl, 2 mM imidazole (pH 7.4), 1 mM DTT, and 5% sucrose with 40–50 $\mu\text{g/ml}$ protein in addition to the indicated Mg^{2+} and nucleotide concentrations. The pulse length was 140 μs at a field strength of ~ 1.2 kV/cm. The signal amplitudes, A_{total} , ΔA_{rise} , and ΔA_{decay} , were extracted directly from the birefringence curves after subtracting the contribution from buffer. The amplitudes and relaxation times of the separate components reported here were extracted from double exponential fits to the decay data.

Myosin	$[Mg^{2+}]$	Nucleotide	$-A_{\text{total}}^2 \delta / (cE^2) \times 10^3$	$-\Delta A_{\text{rise}} \Delta A_{\text{decay}}$	$-A_{\text{fast}} A_{\text{slow}}$	$\langle \tau_{\text{fast}} \rangle^b$	τ_{slow}^b
	<i>mM</i>					μs	μs
Phosphorylated	3	0	5.3 ± 0.4	0.18 ± 0.03	0.28 ± 0.02	12 ± 3	210 ± 20
	3	250 μM ATP	4.7 ± 0.5	0.21 ± 0.05	0.30 ± 0.03	9 ± 3	215 ± 25
	5	0	5.2 ± 0.5	0.18 ± 0.04	0.29 ± 0.03	13 ± 2	220 ± 20
	5	250 μM ATP	5.1 ± 0.5	0.22 ± 0.06	0.32 ± 0.05	8 ± 2	230 ± 30
Dephosphorylated	3	0	2.3 ± 0.3	0.20 ± 0.02	0.30 ± 0.04	12 ± 2	225 ± 15
	3	250 μM ATP	2.4 ± 0.3	0.22 ± 0.05	0.31 ± 0.05	9 ± 3	230 ± 25
	4.5	0	0.25 ± 0.1	0.4 ± 0.1	0.34 ± 0.08	30 ± 12	240 ± 45
	4.5	5 μM ADP	2.1 ± 0.2	0.19 ± 0.03	0.42 ± 0.03	42 ± 5	230 ± 20
	4.5	5 μM AMPPNP	2.2 ± 0.2	0.22 ± 0.04	0.36 ± 0.04	27 ± 5	245 ± 20
	5	250 μM ATP	2.1 ± 0.3	0.21 ± 0.05	0.35 ± 0.06	22 ± 7	235 ± 25

^a The normalized amplitude with δ in radians is given in units of $(\text{mg/ml})^{-1} (\text{kV/cm})^{-2}$.

^b Relaxation times are normalized to water viscosities at 20 °C.

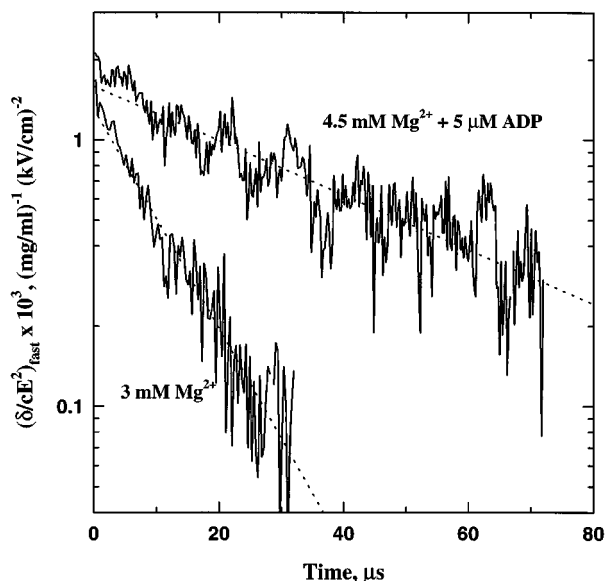


FIG. 6. Effects of Mg^{2+} and nucleotide on the decay kinetics of the fast, positive birefringence component for dephosphorylated minifilaments. Semilog plots for the birefringence decay of the fast component signal are shown for 3 mM Mg^{2+} and for 4.5 mM Mg^{2+} with 5 μM ADP to illustrate the large changes in relaxation time that accompany nucleotide binding. The total signal amplitudes are closely similar for the two conditions shown. The contribution of the slow, negative birefringence component was removed by subtracting the single exponential determined from the best linear fits to the long time data as shown in Fig. 5. The dashed lines are the best linear fits to the data. Other solution conditions were as described in the legend to Fig. 2.

nucleotides have no effect on the electric birefringence of the rods, as expected if nucleotides interact only with S1 heads.

The bending force spring constant of monomers in the minifilament can be estimated (28) from the magnitude of the electric birefringence signal, assuming that the bending is Gaussian and planar and occurs at the HMM-LMM junction and that the S1 heads make little contribution to the birefringence compared with the coiled-coil α -helices of the rest of the molecule. For a bending spring constant α in units of energy/radian² and thermal energy kT , reduced spring constants, α^2 ($= \alpha/2kT$), for dephosphorylated minifilaments at 4–5 mM Mg^{2+} with and without bound nucleotide are estimated as ~ 15 and ~ 300 , respectively. These values correspond to root mean

square angular fluctuations, $\sqrt{\langle \phi^2 \rangle}$, of about 10 and 2°, respectively.

Structural Implications of the Change in Relaxation Time of the Positive Signal—In contrast to the relative insensitivity of τ_{slow} to Mg^{2+} concentration and nucleotide binding, the relaxation time of the fast, positive birefringence component show a substantial dependence on conditions (Table I). Even under conditions that give similar signal amplitudes, the average fast component relaxation times depend significantly on myosin phosphorylation, Mg^{2+} concentration, and nucleotide species.

The decay of the positive birefringence component is through the spinning rotation of the long axis (*cf.* Fig. 1) and therefore is sensitive to the distribution of mass perpendicular to the filament axis, in particular to the angle between S2 rods and the minifilament axis, the angle between S1 and S2, the angle between S1 heads, and S1 conformation. These structural parameters are not as yet well enough characterized to justify hydrodynamic calculations. Given the comparative insensitivity of $A_{\text{fast}}/A_{\text{slow}}$ to experimental conditions (Table I), however, the changes in $\langle \tau_{\text{fast}} \rangle$ likely reflect changes either in S1 conformation or in the orientation of S1 relative to the minifilament axis, rather than in S2. A change in isolated S1 head conformation with nucleotide binding has been observed previously (33–35).

Correlation Between Structural Data and Actin-activated Mg^{2+} -ATPase Activity—We had previously (15) proposed that minifilament stiffness is directly related to enzymatic activity for three reasons: the actin-activated Mg^{2+} -ATPase activity of dephosphorylated myosin II minifilaments is maximally expressed at 4–5 mM Mg^{2+} when the filaments show substantial stiffness; phosphorylation greatly inhibits the actin-activated Mg^{2+} -ATPase activity and simultaneously inhibits the stiffening of minifilaments at 4–5 mM Mg^{2+} ; and the nonlinear dependence of enzymatic activity of minifilament copolymers on the ratio of phosphorylated and dephosphorylated monomers parallels their change in stiffness. The present data require modification of this proposal. In the presence of 5 mM Mg^{2+} and 250 μM ATP, minifilaments of catalytically active, dephosphorylated myosin II are a factor of 10 more flexible than without bound ATP and only a factor of 2 stiffer than inactive, phosphorylated minifilaments. Thus, the present data suggest that enzymatic activity may correlate more closely with the ability of minifilaments to cycle between stiff and flexible conformations coupled to ATP binding, hydrolysis, and subsequent release. This transition between flexible and stiff conformations

is consistent with the large difference in axial compressibility of muscle fibers under rigor and relaxed conditions (36, 37). It is also consistent with recent proposals based on spectroscopic experiments (38, 39) that the myosin structural transition from the weakly actin bound, preforce state (or states) to the strongly bound rigor state is coupled to a dynamically disordered to ordered configurational change.

The substantial differences in $\langle\tau_{\text{fast}}\rangle$ seen with nucleotide binding and myosin phosphorylation are perhaps even more closely linked to enzymatic activity, given the dependence on nucleotide species, *i.e.*, actin-activated Mg^{2+} -ATPase activity may also correlate with nucleotide-dependent conformational changes in S1 or at the S1-S2 junction. Because there is no direct correlation between $\langle\tau_{\text{fast}}\rangle$ and A_{total} , the postulated nucleotide-dependent changes in S1 structure (and enzymatic activity) are not simply or directly coupled to changes in filament flexibility. The nucleotide-dependent conformational changes in S1 inferred from the electric birefringence are entirely consistent with the current model for the cross-bridge cycle but nucleotide-dependent changes in the conformation of the HMM-LMM junction introduce a novel concept that is likely not to be specific to *Acanthamoeba* myosin II.

Concluding Remarks—The coupling of the three experimental observables, A_{total} , $\langle\tau_{\text{fast}}\rangle$, and actin-activated Mg^{2+} -ATPase activity with heavy chain phosphorylation, nucleotide binding, and Mg^{2+} concentration indicates an important role for minifilament flexibility and conformational change in myosin activity. The mechanism for coupling these actions, however, is still obscure. All three are regulated by events at opposite ends of the myosin molecule: phosphorylation at the C-terminal tail and nucleotide binding to the S1 head. It is not clear where Mg^{2+} is acting. Changes in proteolytic susceptibility have also shown that the conformation of the S1 head is coupled to C-terminal phosphorylation (40) and that the conformation of the C-terminal tail is coupled with nucleotide binding to the S1 head (16). Other than that both demonstrate that the opposite ends of the myosin II molecule are linked; however, there is no firm basis for comparing the conformational changes detected by limited proteolysis and those detected by electric birefringence.

REFERENCES

- Mooseker, M. S., and Cheney, R. E. (1995) *Annu. Rev. Cell Dev. Biol.* **11**, 633–675
- Sellers, J. R., and Goodson, H. V. (1995) in *Protein Profile* (Sheterline, P., ed) Vol. 2, 1323–1423
- Rayment, I., Rypniewski, W. R., Schmidt-Bäse, K., Smith, R., Tomchick, D. R., Benning, M. M., Winkelmann, D. A., Wesenberg, G., and Holden, H. M. (1993) *Science* **261**, 50–58
- Trybus, K. M. (1994) *J. Muscle Res. Cell Motil.* **15**, 587–594
- Eden, D., and Highsmith, S. (1995) *Biophys. J.* **68**, (suppl.) 372–373
- Waller, G. S., Ouyang, G., Swafford, J., Vibert, P., and Lowey, S. (1995) *J. Biol. Chem.* **270**, 15348–15352
- Fisher, A. J., Smith, C. A., Thoden, J., Smith, R., Sutoh, K., Holden, H. M., and Rayment, I. (1995) *Biophys. J.* **68**, (suppl.) 19–28
- Irving, M., Allen, T. S. C., Sabido-David, C., Cralk, J. S., Brandmeier, B., Kendrick-Jones, J., Corrie, J. E. T., Trentham, D. R., and Goldman, Y. E. (1995) *Nature* **375**, 688–691
- Côté, G. P., Collins, J. H., and Korn, E. D. (1981) *J. Biol. Chem.* **256**, 12811–12816
- Collins, J. H., Côté, G. P., and Korn, E. D. (1982) *J. Biol. Chem.* **257**, 4529–4534
- Kuznicki, J., Albanesi, J. P., Côté, G. P., and Korn, E. D. (1983) *J. Biol. Chem.* **258**, 6011–6014
- Atkinson, M. A. L., Lambooy, P. K., and Korn, E. D. (1989) *J. Biol. Chem.* **264**, 4127–4132
- Ganguly, C., Atkinson, M. A. L., Attri, A. K., Sathyamoorthy, V., Bowers, B., and Korn, E. D. (1990) *J. Biol. Chem.* **265**, 9993–9998
- Wijmenga, S. S., Atkinson, M. A. L., Rau, D., and Korn, E. D. (1987) *J. Biol. Chem.* **262**, 15803–15808
- Rau, D. C., Ganguly, C., and Korn, E. D. (1993) *J. Biol. Chem.* **268**, 4612–4621
- Redowicz, M. J., Martin, B., Zolkiewski, M., Ginsburg, A., and Korn, E. D. (1994) *J. Biol. Chem.* **269**, 13558–13563
- Collins, J. H., and Korn, E. D. (1981) *J. Biol. Chem.* **256**, 2586–2595
- Collins, J. H., and Korn, E. D. (1980) *J. Biol. Chem.* **255**, 8011–8014
- Côté, G. P., Robinson, E. A., Appella, E., and Korn, E. D. (1984) *J. Biol. Chem.* **259**, 12781–12787
- Collins, J. H., Kuznicki, J., Bowers, B., and Korn, E. D. (1982) *Biochemistry* **21**, 6910–6915
- Pardee, J. D., and Spudich, J. A. (1982) *Methods Enzymol.* **85**, 164–181
- Pollard, T. D., and Korn, E. D. (1973) *J. Biol. Chem.* **248**, 4682–4690
- Provencher, S. W. (1982) *Comput. Phys. Commun.* **27**, 213–227
- Provencher, S. W. (1982) *Comput. Phys. Commun.* **27**, 229–242
- Hammer, J. A., III, Bowers, B., Paterson, B. M., and Korn, E. D. (1987) *J. Cell Biol.* **105**, 913–925
- Highsmith, S., and Eden, D. (1985) *Biochemistry* **24**, 4917–4924
- Highsmith, S., and Eden, D. (1986) *Biochemistry* **25**, 2237–2242
- Rau, D. C. (1993) *J. Biol. Chem.* **268**, 4622–4624
- Eads, T. M., Thomas, D. D., and Austin, R. H. (1984) *J. Mol. Biol.* **179**, 55–81
- Kinosita, K., Ishiwata, S., Yoshimura, H., Asai, H., and Ikegami, A. (1984) *Biochemistry* **23**, 5963–5975
- Ludescher, R. D., Eads, T. M., and Thomas, D. D. (1988) *J. Mol. Biol.* **200**, 89–99
- Redowicz, M. J., Rau, D. C., Korn, E. D., and Hammer, J. A., III (1996) *Biophys. J.* **70**, 160 (abstr.)
- Wakabayashi, K., Tokunaga, M., Kohno, I., Sugimoto, Y., Hamanaka, T., Takezawa, Y., Wakabayashi, T., and Amemiya, Y. (1992) *Science* **258**, 443–447
- Highsmith, S., and Eden, D. (1993) *Biochemistry* **32**, 2455–2458
- Ostap, E. M., White, H. D., and Thomas, D. D. (1993) *Biochemistry* **32**, 6712–6720
- Brenner, B., and Yu, L. C. (1991) *J. Physiol.* **441**, 703–718
- Xu, S., Brenner, B., and Yu, L. C. (1993) *J. Physiol.* **461**, 283–299
- Roopnarine, O., and Thomas, D. D. (1995) *Biophys. J.* **68**, 1461–1471
- Ostap, E. M., Barnett, V. A., and Thomas, D. D. (1995) *Biophys. J.* **69**, 177–188
- Ganguly, C., Martin, B., Bubb, M., and Korn, E. D. (1992) *J. Biol. Chem.* **267**, 20905–20908